View metadata, citation and similar papers at core.ac.uk

brought to you by CORE

provided by IntechOpen

We are IntechOpen, the world's leading publisher of Open Access books Built by scientists, for scientists

4,800
Open access books available

122,000
International authors and editors

135M
Downloads

Our authors are among the

154
Countries delivered to

TOP 1%
most cited scientists

12.2%
Contributors from top 500 universities

CLARIVATE ANALYTICS BOOK CITATION INDEX INDEXED

WEB OF SCIENCE™

Selection of our books indexed in the Book Citation Index in Web of Science™ Core Collection (BKCI)

Interested in publishing with us?
Contact book.department@intechopen.com

Numbers displayed above are based on latest data collected.
For more information visit www.intechopen.com

Chapter 9

Single- and Multiple-Junction p-i-n Type Amorphous Silicon Solar Cells with p-a-$Si_{1-x}C_x$:H and nc-Si:H Films

S. M. Iftiquar, Jeong Chul Lee, Jieun Lee, Juyeon Jang, Yeun-Jung Lee and Junsin Yi

Additional information is available at the end of the chapter

http://dx.doi.org/10.5772/51732

1. Introduction

The p-a-$Si_{1-x}C_x$:H alloy is popularly knows as a wide band gap semiconducting alloy. It was demonstrated in the 1980s that application of the p-a-$Si_{1-x}C_x$:H alloy leads to improved performance of a solar cell with better blue response of its quantum efficiency (QE) [1]. There are few other well known wide band gap alloy materials available, however one interesting advantage of the p-a-$Si_{1-x}C_x$:H is that both the C and Si are four fold coordinated atoms, and hence a suitably prepared material may attain wider optical gap with good stability.

The p-i-n type diodes have been widely used in photovoltaic solar (PV) energy conversion. Incident light that falls on the diode is absorbed in the intrinsic layer and electron-hole (e-h) pairs are generated, producing the PV or electrical energy, while the p-type and n-type layers produce built-in electric field to separate the e-h pairs, created in the i-type layer. Recently the interest on PV energy has been growing because it can provide clean energy. However, the efficiency of a solar cell is lower than that is expected, although there is a continuous improvement in solar cell efficiency (η) throughout the history of solar cell. One of the reasons for such a low efficiency has been loss of light at the front surface of the cell due to reflection, as well as part of the low energy photons remains unabsorbed in the cell. Thus, for a maximum utilization of the incident light for PV energy conversion, the structural and material properties are expected to play some important roles. Light absorption at the doped window layer is also considered loss of light.

Another challenge is the material and interface defects that can hinder the collection of the photo generated e-h pairs [2]. This defect can exist in the material or at the interface [3,4]. Reducing such defects is also one of the priorities of a solar cell fabrication. The collection of

INTECH
open science | open minds

© 2012 Iftiquar et al.; licensee InTech. This is an open access article distributed under the terms of the Creative Commons Attribution License (http://creativecommons.org/licenses/by/3.0), which permits unrestricted use, distribution, and reproduction in any medium, provided the original work is properly cited.

the e-h pairs can also depend upon built-in electric field created by doped p-type and n-type layers [5], and thus degree and efficiency of doping of these layers are also important.

Along with its wider optical gap, the doped window layer or the top p-layer is generally made thinner as well [6], so that more light can enter into the active region of the device. However, with a thinner p-type layer the output voltage also get reduced [7,8], leading to more recombination loss of the photo generated charge carriers. Similarly, if optical gap of the window layer is high, then also the absorption loss at the p-type layer reduces. So, a wider optical gap thicker p-type layer appears to be a good option for a solar cell window layer. However, it is known that with increased carbon content within the material, optical gap increases [9,10] and the wider optical gap is usually associated to lower dark conductivity [11], and higher activation energy (E_a). As a result the higher optical gap of the p-type layer may lead to lower output voltage from the device.

There are several different types of window layer one can use, like hydrogenated amorphous silicon oxide (a-SiO:H) [12], hydrogenated amorphous silicon carbide (a-$Si_{1-x}C_x$:H) [1,13], hydrogenated amorphous silicon (a-Si:H) [14] etc and micro-crystalline or nano-crystalline version of these materials. Out of these, wide band gap a-$Si_{1-x}C_x$:H and nc-Si:H materials are two of the most promising materials.

Being amorphous in nature and containing hydrogen (H) and carbon (C) atoms in the material the composition and local bonding structure of the characteristic property of the material is thus partly determined by microstructure within the material. A microstructure is a local non-uniformity of the material, and is generally used to indicate the density of SiH_n or CH_n type poly-hydrides in the material, where $1 \leq n \leq 3$. Such a microstructure can also be called a void structure as well, that may be deteriorative for the material [15,16].

The carbon-silicon bonds lead to higher optical gap of the material and thus the increased carbon fraction x in a-$Si_{1-x}C_x$:H leads to higher optical gap of the material [1,9,17,18]. This higher optical gap results in higher optical transparency of the material, making it more suitable for a transparent window layer of a p-i-n type solar cell. It is also known that boron doping of amorphous silicon alloy material leads to reduction in optical gap [19]. Thus, a suitable boron doped p-a-$Si_{1-x}C_x$:H can become one of the best suited window layers.

In a multiple- junction amorphous silicon solar cell, multiple p-i-n type structures are joined in tandem [20]. The multiple junction solar cells are also known as multi-junction solar cell. The advantage of such a solar cell is that the open circuit voltage (V_{oc}) becomes higher, and a wider spectral range of solar radiation can be absorbed in aggregate to the component cells. In this respect double (DJ) and triple junction (TJ) cells have been extensively studied in recent past [21-24]. As purpose of the DJ or TJ cell is the PV energy conversion by utilizing a wider spectral range, so tailoring of the band gap of the component cells become very important part of the design. In a suitable design, the top cell should have wider optical gap so that shorter wavelength light can be absorbed but the longer wavelength light will remain unabsorbed, while the middle cell should absorb the middle part and the bottom cell should absorb the longer wavelength part of the solar spectra. Thus, for the single p-i-n type cell or multiple-junction cell, a wide band gap window layer becomes a very significant component of the device.

http://dx.doi.org/10.5772/51732

Hydrogenated nanocrystalline silicon (nc-Si:H) thin film is also known as hydrogenated microcrystalline silicon (μc-Si:H) thin film. It is composed of amorphous phase and a few nm sized crystalline Si grains [25-27]. The p-type nc-Si:H is also a promising material for solar cell window layer [28] The nc-Si:H thin films have optical bandgap of around 1.1 eV, unlike the a-Si:H thin films that have band gap of about 1.7eV. Light induced degradation of nc-Si:H films are low [29, 30]. Having lower optical gap of this nc-Si:H films, it is possible to utilize longer wavelength radiation of solar spectra. The nc-Si:H has lower optical band gap and higher absorption coefficient of longer wavelength light, for which it can be used in the bottom cell of a multiple-junction solar cell, preceded by a wider band gap top cell. Such a combination of amorphous and micro-crystalline cells can be called as a micromorph solar cell [31-32]. In a micromorph solar cell, the bandgap of the top cell is ~ 1.7eV and that of bottom cell is 1.1eV. Usually the thickness of a-Si:H top cell is thinner than a usual single p-i-n type cell. The thickness of the intrinsic layer of nc-Si:H layer is almost 10 times to that in the a-Si:H top cell [20].

Furthermore, tunneling and recombination junctions (TRJs) are necessary in a MJ cell [33]. In a p-i-n type MJ cell, multiple unit cells are joined in tandem. This leads to a junction between n-type layer of the top cell to the p-type layer of the bottom one (or p-n junction), that may act as a recifying diode placed opposite to the p-i-n cell. This may be deteriorative to cell performance. Using a TRJ type p-n junction is a solution to the problem, without this the performance of a MJ cell remains poor.

Thus, we try to explore various aspects of fabricating single and multiple junction thin film solar cell, and characterize their performance.

2. Experimental

2.1. Deposition of Silicon Alloy Films

We prepared amorphous type p-a-$Si_{1-x}C_x$:H, a-Si:H, n-a-Si:H and nano-crystalline p-nc-Si:H, i-nc-Si:H, n-ncSi:H films, characterized them and applied in single junction, double junction and triple junction solar cells. We used RF PECVD, VHF PECVD, HW-CVD, for depositing silicon alloy materials, sputtering for AZO film deposition and thermal evaporation for metal electrode deposition. The silane (SiH_4), methane (CH_4), hydrogen (H_2), diborane (B_2H_6) (1% in H_2), phosphine (PH_3)(1% in H_2) were the source gases for various films, where the SiH_4, CH_4, H_2 were used for a-$Si_{1-x}C_x$:H alloy materials, SiH_4, H_2 for a-Si:H and nc-Si:H films, B_2H_6 was used as a p-type dopant gas and PH_3 as the n-type dopant one.

The p-a-$Si_{1-x}C_x$:H films were deposited by 13.56 MHz RF PECVD with CH_4, SiH_4, H_2, B_2H_6 source gases, at substrate temperature (T_s) of 200°C. For optoelectronic characterization, the films were deposited on 25mm×25mm sized Corning 1737 glass substrates and for Fourier transform infra red (FTIR) spectroscopic study we used (100) oriented p-type c-Si wafers. Later, selective samples are used for the p-type layer of the p-i-n type solar cells. Prior to film deposition the substrates were cleaned in acetone, methanol and de-ionized water. A 10^{-8} Torr base pressure of the reaction chamber was maintained prior to the film depositions.

The intrinsic a-Si:H and nc-Si:H absorption layers were deposited by 60MHz VHF PECVD and Hot Wire CVD methods. Deposition condition for one of the i-type layers is, H_2 flow rate 60 sccm, SiH_4 flow rate 7 sccm, RF power 8 Watt, pressure 300 mTorr. Deposition condition for n-type layer is, H_2 flow rate 10 sccm, SiH_4 flow rate 5 sccm, PH_3 flow rate 1% to that of silane, RF power 6 Watt, pressure 300 mTorr. Thickness and optical gap of i-type layer is maintained at ~200 nm and 1.75 eV, and that of n-type layer at ~30 nm and 1.7 eV respectively.

Electrical characteristics of the thin films were measured in a planar electrode configuration. Auger analysis was performed in order to estimate fractional carbon content (x) of the material.

2.2. Deposition of intrinsic nc-Si:H thin film by 60MHZ VHF CVD

Table 1 shows the deposition conditions of nc-Si:H thin film. The nc-Si:H films were prepared at higher hydrogen dilution.

H_2(sccm)	60 ~ 185
R_{Si}	10.4% ~ 3.6%
T_s.(°C)	140°C & 200

Table 1. Deposition condition of nc-Si:H films at various hydrigen dilution, $R_{Si} = SiH_4/(SiH_4+H_2)$, with SiH_4 flow rate as 7 sccm, RF power 8Watt, deposition time 60 min, d_{sh} =2cm that is the electrode seperation of the PECVD system.

2.3. Characterization of Si alloy films

Raman and spectroscopy and X-ray diffraction (XRD) spectroscopy were used to characterize crystallinity of the films. Usually the nanocrystals were embedded in amorphous silicon phase and thus the characteristic spectra of both the crystalline and amorphous phase is visible in the spectroscopic analysis. The Raman spectra of nc-Si:H silicon thin film is composed of 520cm^{-1} peak (of intensity I_c) of crystalline phase and 480cm^{-1} peak (of intensity I_a) of amorphous phase [27]. In polycrystalline silicon thin film, the peak is shifted to lower wavenumber because of the amorphous phase and occurs at 517-518cm^{-1}. The crystalline volume fraction (X_c) was calculated using relation [28, 34, 35]

$$X_c = (I_c)/(I_c + I_a) \tag{1}$$

The average crystal size was obtained from

$$d_{Raman} = 2\pi\sqrt{B/\Delta\omega} \tag{2}$$

where $\Delta\omega$ is the shift of Raman peak for μc-Si:H with respect to that of c-Si, B=2.0cm^{-1}.nm^2 [36]. The dark conductivity (σ_d) and photoconductivity (σ_{ph}) were measured for the films de-

http://dx.doi.org/10.5772/51732

posited on the glass substrates, with planar electrode configuration. The photoconductivity was measured under AM1.5 (100mW/cm^2) light generated by solar simulator. The hydrogen content C(H) as well as hydrogen bonding configurations of the films were estimated by FTIR spectroscopy [37]. The hydrogen content can be obtained from the absorption peak at 640 cm^{-1} that includes the rocking mode of bonded hydrogen. To get absorption strength $\alpha_{640}(\omega)$ of rocking mode, absorption peak at 640 cm^{-1} is fitted to a Gaussian function. From the fitted function, the hydrogen content was calculated, using the following equation.

$$C(H) = A_{640} I_{640} \tag{3}$$

$$I_{640} = \int \frac{\alpha_{640}(\omega)}{\omega} d\omega \tag{4}$$

Where A_{640} is a constant needed to calculate hydrogen content from rocking mode, and I_{640} is the integrated absorption coefficient.

2.4. Fabrication of solar cells

Textured TCO coated glasses were used for fabrication of p-i-n type solar cells. After the deposition of the p-, i-, n-type layers, either the solar cell was completed by depositing Ag electrodes or aluminum doped zinc oxide (AZO) layer was deposited by RF magnetron sputtering and then Ag layer was deposited. This AZO/Ag layer combination works as a good back reflector (BR). In order to achieve clear electrical connection the cell was wet etched using HCl (for removal of AZO in the BR) and by reactive ion etching in CF_4 plasma.

The p-type window layer of the cell was tested with various p-a-$Si_{1-x}C_x$:H materials and p-nc-Si:H. In multiple- junction cell we used intrinsic a-Si:H as well as nc-Si:H materials.

For the single p-i-n type a-Si:H solar cell, 8 ~ 20nm thick p-a-$Si_{1-x}C_x$:H was used as p-type layer and to anyalize the interface characteristics with front TCO, p-type nc-Si:H thin film was also inserted between TCO and p-a-$Si_{1-x}C_x$:H layer [38] and improved performance of the solar cell was observed. For the p-i-n nc-Si:H solar cell, about 15nm thick nc-Si:H was used as p type window layer to minimize the band mismatching with i-type nc-Si:H layer. The a-Si:H/nc-Si:H double junction (DJ) cell and a-Si:H/nc-Si:H/nc-Si:H triple junction (TJ) solar cells were also fabricated. To improve performance of the multiple-junction solar cells the tunnel junction in the form of n-nc-Si:H/p-nc-Si:H or n-a(nc)-Si:H/AZO/p-nc-Si:H structures were used.

2.5. nc-Si:H bottom cell using 60MHZ VHF CVD

The nc-Si:H bottom cells were separately fabricated in the form of a single p-i-n type cell structure, measured its characteristic properties and then a few of the selected cells were used in multiple-junction solar cells. Fig. 1 shows the schematic diagram of a nc-Si:H thin film solar cells. Unlike the a-Si:H solar cells, p-type nc-Si:H thin film was used as a window layer to mini-

mize the interface defects arising from the band mismatch with i-nc-Si:H. To form p type nc-Si:H thin film by 13.56 MHz PECVD, higher H_2 gas flow rates were used (see Table 2).

	p nc-Si:H	i nc-Si:H	n a(nc-Si):H
SiH_4(sccm)	0.2 ~ 1	~ 7	5
H_2(sccm)	~ 180	~ 95	5
B_2H_6(sccm)	~ 1	-	-
RF power (W)	16	16	6
Pressure (mTorr)	500	300	300
Thickness	30nm	2μm	30nm

Table 2. Deposition condition for a nanocrystalline single p-i-n type solar cell in a RF PECVD system, with 0.36cm^2 cell area. For BR and back electrode, a 100nm AZO and 500 nm Ag/Al metal layers were deposited at the back of the cell. The n-layer was doped by 1% with phosphine.

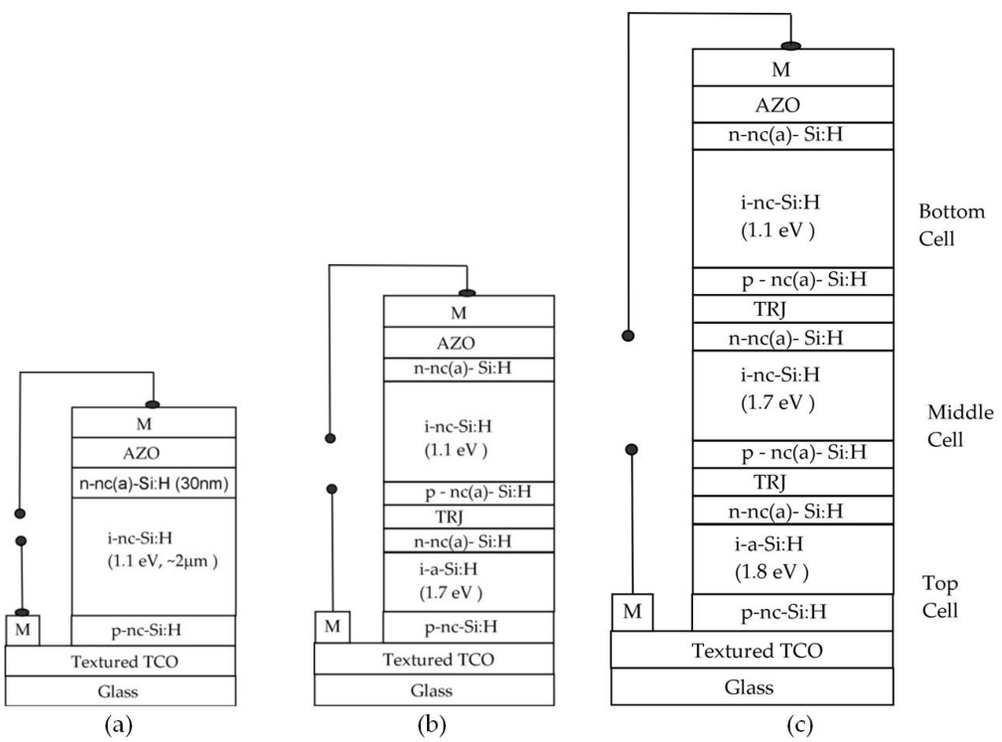

Figure 1. Schematic diagram of (a) single p-i-n type (b) double junction, (c) triple junction solar cell, where M stands for metal electrode.

For n-type layer of the cell, a-Si:H or nc-Si:H thin film was used. The AZO(~100nm) was deposited by RF magnetron sputtering and Ag/Al metal layers were deposited by thermal evaporation. The Al in back reflector (BR) electrode also acts as a protection layer to minimize the damage on Ag during electrode isolation dry etching. The fabricated solar cell areas were 0.36cm^2. The area is controlled by using shadow mask during electrode deposition.

http://dx.doi.org/10.5772/51732

2.6. Structure and fabrication of multiple- junction solar cell

Fig. 1(b) shows the schematic diagram of a double junction and Fig. 1(c) shows that of a triple junction solar cell. Fluorine doped tin oxide (FTO) coated glass (Asahi-U type glass) or textured AZO was used for solar cell front electrode and over which the cells were deposited. P-I-N a-Si:H top and nc-Si:H bottom cells were deposited in turn in multi-chamber system. For the tunnel junctions at the n-p interface, it was made either nano crystalline or AZO layer was deposited in between the n-type and p-type layers of the successive cells as n/AZO/p.

Fig. 1(c) shows the structure of a-Si:H/nc-Si:H/nc-Si:H triple junction thin solar cell. The deposition conditions are given in Table 3 for double junction cell and Table 4 for a triple junction cell. The thickness of a-Si:H top intrinsic layer was 150nm, the thickness of nc-Si:H middle absorption layer was 2.0μm and thickness of bottom absorption layer was 3.2μm. No inter-layer for TRJ was used between the cells and to improve the tunnel junction, the nanocrystalline (n-nc-Si:H)-(p nc-Si:H) layers were used. For back electrode, AZO/Ag BR was used. For a MJ solar cell, current matching is an important step for optimization of device performance. We optimized the component cell structures with the help of QE spectra, after which the i-layer thickness of the middle and bottom cells of a triple junction (TJ) solar cells were kept as 2.0 μm and 3.2 μm respectively.

a-Si:H top-cell				
	p nc-Si:H	**p-a-$Si_{1-x}C_x$:H**	**i a-Si:H**	**n a-Si:H**
SiH_4(sccm)	1	6	7	5
H_2(sccm)	180	5	60	5
B_2H_6(sccm)×100	0.4	1-4	-	-
RF power (W)	16	6	8	6
Pressure (mTorr)	500	300	300	300
Thickness	<5nm	20nm	100-300nm	20-30nm
nc-Si:H bottom-cell				
	p nc-Si:h	**i nc-Si:H**		**n a-Si:H**
SiH_4(sccm)	1	5		5
H_2(sccm)	180	95		5
RF power (W)	16	16		6
Pressure (mTorr)	500	300		300
Thickness	20nm	1.7 μm		20-30nm

Table 3. Deposition condition for a double junction solar cell. The top cell was deposited with textured front TCO, CH_4 flow rate for p-a-$Si_{1-x}C_x$:H as 16 sccm, 1% gas phase doping of n-type layer with PH_3. The bottom cell's p-type layer was 0.4% doped with B_2H_6, with no CH_4 flow and the n-layer as 1% doped. With AZO/Ag as BR, and less than 10nm thick AZO interlayer as a tunnel junction in between n-type and p-type layers of the cells.

a-Si:H top-cell			
	p-a-$Si_{1-x}C_x$:H	**i a-Si:H**	**n nc-Si:H**
SiH_4(sccm)	6	7	2
H_2(sccm)	5	60	150
RF power (W)	6	8	16
Pressure (mTorr)	300	300	500
Thickness	20nm	150nm	20-30nm
nc-Si:H middle-cell			
	p nc-Si:h	**i nc-Si:H**	**n nc-Si:H**
SiH_4(sccm)	1	5.5	2
H_2(sccm)	180	95	150
Pressure (mTorr)	500	300	500
Thickness	20nm	2.0 ηm	20-30nm
nc-Si:H bottom-cell			
	p nc-Si:h	**i nc-Si:H**	**n a-Si:H**
SiH_4(sccm)	1	5.5/6.0/6.5	2
H_2(sccm)	180	95	150
Pressure (mTorr)	500	300	500
Thickness	20nm	3.2 ηm	20-30nm

Table 4. Deposition condition for a triple junction solar cell. All the n-layers of the cells were 1% doped with PH_3, p-layers of the bottom and middle cells were 0.4% doped, The top cell was deposited with textured front TCO, CH_4 flow rate for p-a-$Si_{1-x}C_x$:H as 16 sccm. The p-type layer of the middle and the bottom cells were deposited with 0.4% B_2H_6 doping, no CH_4 flow and the n-layer as 1% doped. With AZO/Ag BR, and less than 10nm thick AZO interlayer as a tunnel junction in between n-type and p-type layers of the cells. For the middle and the bottom cells the RF power was 16W for the p-, i-, n- layers. The cell area was 0.36cm^2.

3. Results and Discussions

3.1. p-a-$Si_{1-x}C_x$:H

Initially we deposited, characterized and optimized the p-type layer, where the diborane flow rate with reference that of silane, DBFR = B_2H_6/SiH_4 that was almost always kept at 0.17 % unless otherwise specified. In the following we discuss preparation and properties of boron doped p-a-$Si_{1-x}C_x$:H films, and then its application to solar cell.

It is known that with increase in methane flow rate the carbon incorporation into the film increases linearly [39]. Fig. 2(a) shows the change in the carbon content of deposited p-a-$Si_{1-x}C_x$ thin film depending on the gas flow ratio y=$CH_4/(CH_4+SiH_4)$. The Fig. 2(a) shows that while the methane flow ratio increases from 0.6 to 0.9, the carbon content x increases almost linearly from 0.1 to 0.3, where the x can be expressed as

http://dx.doi.org/10.5772/51732

$$x = 0.59y - 0.23 \quad (5)$$

for this range of y. The expression for x comes from the linear fit to the data points of Fig. 2(a). It may appear that while methane flow rate is zero the fractional carbon content will become negative. This conclusion is not realistic. The negative intercept of the linear equation (or -0.23) may indicate the change in chemical kinetics, that comes into play in the chemical vapor of the RF PECVD system in presence of methane, in comparison to when methane was absent.

Optical gap (E_g) of the films were measured as the photon energy at which absorption coefficient is 10^4 cm^{-1}. Fig. 2(b) shows the change in the E_g of p-a-Si_{1-x} C_x depending on the C content. The band gap of p-a-Si_{1-x} C_x deposited ranges within 1.7 ~ 2.3 eV. It can be seen that E_g increases almost linearly with x, where

$$E_g = 1.40 + 2.99x \quad (6)$$

The expression for E_g comes from the linear fit to the data points of Fig. 2(b). It may appear that for a-Si:H samples, where carbon content x=0 the optical gap of the sample will be 1.40 eV. However this not the case, as it is known that E_g of a-Si:H is ~1.7 eV and depends on hydrogen content. The reason may be the role played by carbon in amorphous network. At low carbon content of p-a-$Si_{1-x}C_x$:H samples, the number density of Si-H bonds decrease. In a-Si:H sample it's the Si-H bonds that helps enhancing optical gap. In p-a-$Si_{1-x}C_x$:H samples it has been found that Si-H bond density decreases and C-H bond density increases. Thus while carbon content of the p-a-$Si_{1-x}C_x$:H films were increased role of the Si-Si bonds on optical gap that remain unchanged, while number density of Si-H and C-H changes. Thus the role of bonded Si-H, C-H bonds on optical gap may be reflected in the factor 2.99x while the contribution of Si-Si bonds on the optical gap may be contributing to the 1.40 constant of the equation for E_g.

Fig. 2(c) shows effect of C content on the dark conductivity and the related activation energy. The σ_d and activation energy (E_a) were related by Arrhenius relation

$$\sigma_d = \sigma_0 \exp\left[-E_a / kT\right] \quad (7)$$

where σ_0 is a constant, k-Boltzmann constant, T temperature. E_a is estimated experimentally through slope of a plot of $\log(\sigma_d)$ vs 1/T in 25°C to 125°C temperature range. We observed that as x increases, the dark conductivity decreases from 10^{-5} to 10^{-10} Scm^{-1} and the activation energy increases from 0.35 to over 0.8 eV. For p-type material the activation energy is the energy difference between Fermi level and valence band mobility edge. Furthermore, the relatively higher value of activation energy of the samples may be because of lower doping, which is 0.17%, whereas normal doping used in solar cell is usually 1%. However, the trend in variation of E_a and σ_d becomes qualitatively obvious as the trend of the traces were nearly complementary to

each other; meaning increased activation energy and decreased conductivity were similar in nature with activation energy in linear scale while the conductivity in log scale.

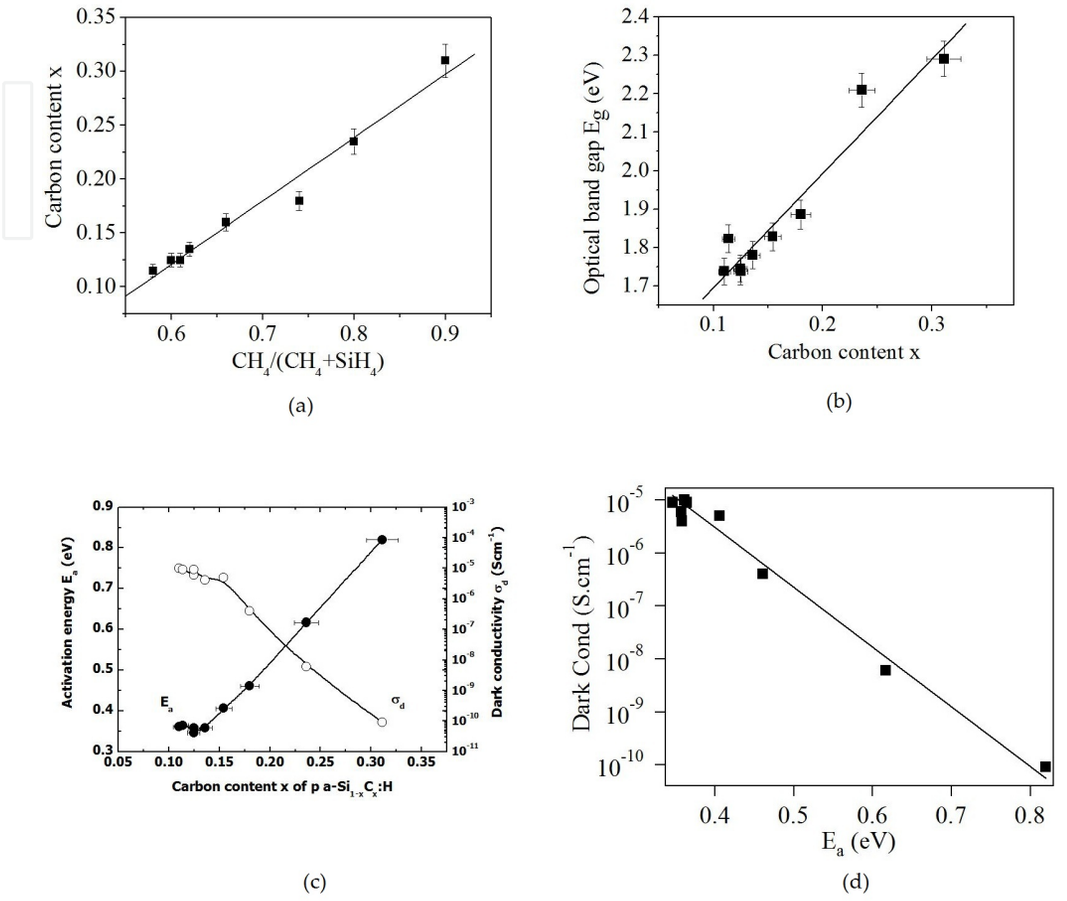

Figure 2. p-a-$Si_{1-x}C_x$:H material characteristics. Variation of (a) x with methane flow rate, (b) optical gap with x, (c) E_a with x, (d) dark conductivity with E_a.

Fig. 2(d) shows the data points for samples with respective E_a and σ_d. The fitting line is an exponential fit, following Arrhenius relation. It shows that the measured dark conductivity and E_a were related by Arrhenius relation. Furthermore it can also be seen from Fig 2(c) that the change in dark conductivity and respective increase in the activation energy are slower for x increasing from 0.10 to ~0.15, whereas Fig. 2(b) shows a nearly linear increase in optical gap with increase in x from 0.10 to 0.32. These materials were p-type, so electrical conduction is mostly contributed by movement of holes and activation energy is the energy difference between the Fermi level and valence band mobility edge. Usually, when optical gap increases with alloying of Si with other atoms both the valence and conduction band mobility edges move apart. The weaker correlation between the increase in optical gap and change in dark conductivity activation energy may indicate that the optical gap enhancement may be controlled by C-H rich phase of p-a-$Si_{1-x}C_x$:H material [17, 40] while electrical conduction is mainly due to silicon rich phase. Thus, although optical gap was enhanced due to C-incorporation into the a-Si network yet the presence of increased C-H bonds does not impede the

http://dx.doi.org/10.5772/51732

electrical conduction (for 0.1<x<0.15) through Si-Si bonds through Si-rich phase of the material. Thus it appears x= ~0.15 is a suitable alloy composition because the E_a remains low even though optical gap as well as σ_d is relatively high. A similar trend in intrinsic a-$Si_{1-x}C_x$:H has been observed [9] in which the photo conductivity, carrier mobility and lifetime remains nearly unchanged for x~0.15, and for x>0.15 it reduces faster. Thus it is quiet reasonable to consider x~0.15 is optimum compositional ratio for amorphous silicon carbide alloy.

3.2. P-type Layer Activation Energy

Fig. 3(a) shows maximum resistance at TCO/p-type layer interface, the fill factor and open circuit voltage of p-i-n-type a-Si:H solar cell, while the activation energy of the p-type layer increases and fill factor of the cell decreases. So the cell parameters become poorer at higher E_a.

At higher x resistivity of the film, activation energy increases and hence the resistance at the TCO/p-interface as well as that of the p-type layer was also higher. Higher activation energy of the p-type layer leads to reduction in energy difference between the Fermi levels of p-type and i-type layers that ultimately leads to reduction in V_{oc} of the cell. The higher E_a is associated to lower conductivity, that in this study, played a role to lower FF, J_{sc} and V_{oc}.

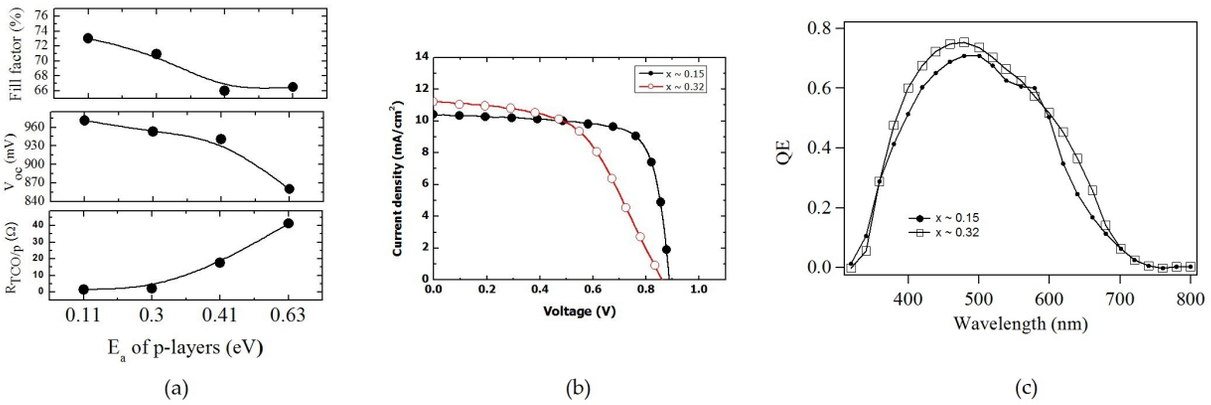

Figure 3. (a) Dependance of TCO/p interface resistance, FF, V_{oc}, on E_a of the p-layer. And variation of (b) I-V characteristic curve (c) QE with x.

Light induced current voltage (LIV) characteristics is shown in Fig. 3(b). From the LIV characteristics it appears that at x=0.32 the short circuit current density (J_{sc}) is higher. This may be because of better quantum efficiency of cell as compared to the cell with p-type layer having carbon content x =0.15. Increased J_{sc} can be observed when larger number of photons enter into the i-type layer and creates increased electron-hole pair. For x=0.32 optical gap of the p-type layer is ~2.3 eV and thus a larger number of photons can pass through the p-type layer.

From the I-V curve in Fig. 3(b), it can be seen that while the voltage across the cell was <0.5 Volts the current delivered by the cell was higher than the other cell, and the current remained lower in this cell if the voltage higher than 0.5 Volts, ultimately leading to lower V_{oc}. Such a situation may be possible if localized mid-gap defects at the p-i interface remains high. What may happen is when the cell is short circuited or V< 0.5 Volts, the photo-generat-

ed e-h pairs were rapidly collected by the external circuit and thus most of the e-h pairs produce higher photo-generated current from the cell. Whereas, while V>0.5 Volts the average residual time for e-h pairs inside the cell increased, leading to a higher possibility of the charge carriers being trapped at the defect states and lost. Such a model can be true if defect states created by C incorporation is ~0.5 eV above the quasi-Fermi level for holes, which may be ~0.85 eV above the valence band mobility edge. We estimate location of the defect states as 0.85 eV by adding E_a =0.35 eV for x=0.15 and the 0.5 eV. Fig. 2(c) shows that activation energy of the p-a-$Si_{1-x}C_x$:H layer for x=0.32, is 0.82 eV, which is very close to the 0.85 and thus the role of midgap defect states become more obvious at higher carbon incorporation. In this situation it leads to lower FF and V_{oc}. So the shunt resistance (R_p) of the cell (with x=0.32) becomes lower than the other cell (with x=0.15).

Thus a model of increased interface defects for x~0.32 may also be supported to some extent from the quantum efficiency measurements. As it is well known that absorption coefficient of amorphous silicon alloy films increase with reduction in wavelength of incident photon. Thus shorter wavelength photons will have a smaller penetration depth from the surface of incidence. In QE measurements, Fig. 3(c), when wavelength of incident radiation was gradually reduced the electron-hole pair generation takes place closer to the p-i interface. It can be seen from Fig. 3(c) that 360 nm wavelength the EQE of the cell with the x~0.18 was same to that with cell with x~0.32. It can be assumed that at this wavelength the photo generated e-h pairs were created at the edge of p-i interface. So when the incident photon energy was lower than the above critical wavelength, the EQE became lower, as the e-h pairs were generated at the defective interface region.

Thus, it seems that at higher carbon incorporation the p-i interface as well as TCO/p-type layer interface the defects increased that lead to poorer performance of the cell.

Although there are several disadvantages for samples with higher x, yet its advantage is better transmission of higher energy photons into the i-type layer of the cell and hence generating electron-hole pairs with shorter wavelength light, as shown in Fig. 3(c). It shows better external quantum nearly at all wavelength except below 360 nm.

At higher level of boron doping the activation energy falls significantly [41]. However, it is known that with the increased boron doping optical gap of the material falls [42] and this is a regular feature.

3.3. P-type Layer Thickness

We have observed that with a thin p-type layer, the cell performs better. We have observed that the open circuit voltage decreases as the thickness of p-a-$Si_{1-x}C_x$:H decreases especially when it is below 10nm. We also observed that V_{oc} does not change much for p-type layer thickness more than 12nm. So optimized thickness of the p-type layer can be considered as 10 nm. It is also obvious that at higher sample thickness optical transmission through the film lowers. Urbach energy of a-$Si_{1-x}C_x$:H films increase from ~50 meV with increased optical gap and is expected to saturate around 90 meV at optical gap higher than 2.1 eV [43]. The FF continuously decreases with increased thickness of the p-type layer.

http://dx.doi.org/10.5772/51732

We have also observed an improved blue response of cell at lower p-type layer thickness. One simple reason is the Beer Lambert's law of absorption $I_T = I_0 \exp[-\alpha d]$, where I_T is intensity of transmitted light through a material layer of thickness d having absorption coefficient α, I_0 is intensity of incident light. Thus with a thicker (higher d) p-a-$Si_{1-x}C_x$:H layer the light penetrating though the p-type layer will be lower. We have observed that the maximum available quantum efficiency of the cell also decreases with increase in thickness of the p-type layer.

Thus, at increased thickness of p-type layer, intensity of transmitted light decreases leading to lower J_{sc} and lower quantum efficiency. Increased thickness also indicates higher electrical resistance across the p-type layer and thus reduced FF as well as efficiency. Whereas at reduced thickness (<8nm) of the p-type layer the formation of p-type layer remains insufficient and enough built-in field is not generated.

This result is similar to that observed by Myong et. al., [8] and Lee et al [44] that at lower p-type layer thickness the quantum efficiency of the cell at shorter wavelength improves while efficiency, short circuit current density FF etc improves at the beginning but decreases at higher p-type layer thickness.

3.4. Effect of Hydrogen Dilution

We have observed that the higher hydrogen dilution for the p-type layer deposition over the TCO, leads to defective TCO/p interface, mostly due to the chemical reduction of the top surface of the TCO.

Use of hydrogen dilution during deposition is an important step for defect reduction of deposited films. However, while the same technique is used for solar cell fabrication, specially for deposition of p-type layer, unless caution is maintained it leads to cells with poorer performance. During the p-layer deposition, if higher H-dilution was used the V_{oc} and J_{sc} reduces. At higher hydrogen dilution (R), the H-radicals in the plasma might have eroded top surface of the TCO by chemically reducing it through removal of part of bonded oxygen.

It is known that at higher hydrogen dilution the characteristics of intrinsic a-$Si_{1-x}C_x$:H films improves, like its conduction band Urback energy decreases and carrier life time increases [45] yet during device fabrication with TCO, the situation changes and one faces limitation in using higher hydrogen dilution that risks deteriorating top surface of the TCO. Our results are similar to that of Tawada et al. [46] however the V_{oc} in our sample is higher may be because of improved band gap matching at p-type and i-type layers and lower interface defects.

Although optimization of cell performance has been carried out, yet there is possibility to further improve the J_{sc}, cell efficiency etc. by optimization of the cell structure.

3.5. Nano crystalline Silicon and application in Solar cell

As the ratio of SiH_4 gas R_{Si}, increases from 3.5% to 8.0%, the deposition rate increases from 0.9Å/sec to 1.7 Å/sec. At a higher hydrogen flow rate, the film deposition rate reduces due to selective etching of amorphous silicon phase by energetic hydrogen radicals, and thus, crys-

tallinity of the film increases. At a higher hydrogen flow rate, the hydrogen atoms may act as etchant to remove the amorphous silicon phase [47, 48].

Fig. 4(a) shows the Raman characteristics of the above described films. These films, that were deposited with R_{Si} in between 3.6% and 4.5%, were nc-Si:H films. The transverse optic (TO) mode was observed around 520cm^{-1} indicating the presence of nano crystallites in the film. When the R was greater than 4.5%, a broad peak around 480cm^{-1} was observed indicating the presence of an amorphous phase. The crystalline volume fraction of thin films deposited with the ratio of 3.6% and 4.5% is found to be 70% and 52% respectively, the other films show amorphous character.

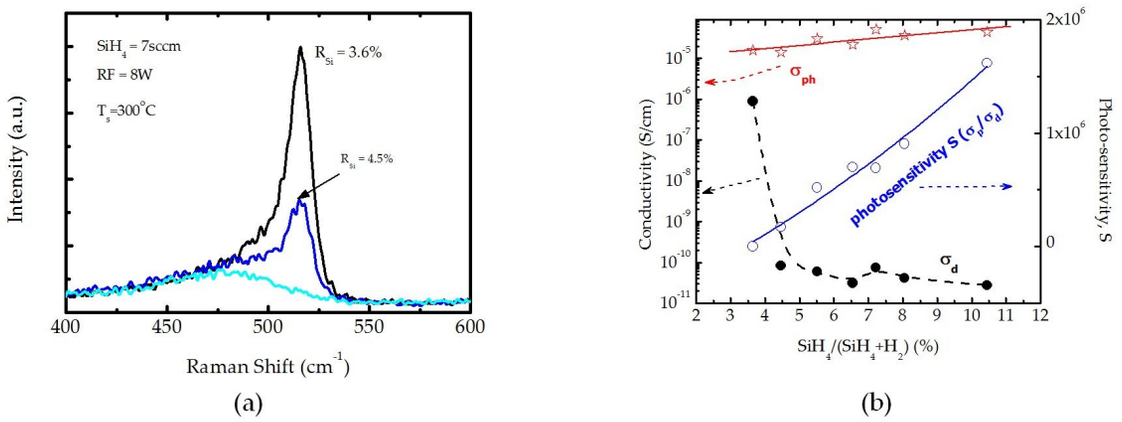

Figure 4. (a) Raman spectra and (b) electrical conductivities of the films prepared at various silane flow rates R_{Si}.

Fig. 4(b) shows the electrical characteristics of nc-Si:H thin film deposited with varying R_{Si}. The σ_d of the film deposited with the ratio of 3.6% is 10^{-6}S/cm. When the flow ratio was increased more than that, the dark conductivity rapidly reduced to 10^{-10}S/cm. Generally, an amorphous silicon thin film lower defect density and hence a lower dark conductivity. However, when transition from amorphous to nanocrystallinity occurs, crystalline grains were formed and the amorphous phase exists in defective grain boundary. Thus, the amorphous silicon films show lower dark conductivity in comparison to nanocrystalline silicon.

Unlike the dark conductivity (σ_d), the photo-conductivity (σ_{ph}) did not change much with nano-crystallinity, and remains around 1×10^{-4}S/cm, Fig. 4(b). Thus the photo-sensitivity was high for the a-Si:H films in comparison to that of the nc-Si:H films.

3.6. Analysis of nc-Si:H thin film dependence on substrate temperature

Another important parameter that affect the nano-crystallinity of the nc-Si:H thin film is the substrate temperature [49]. Fig. 5(a) shows the Raman spectrum of the films as the substrate temperature was varied. The films formed at 100℃ and 140℃ temperature, were amorphous. Nano-crystalline films were observed when the T_s was above 200℃. The crystalline volume fraction increased from 55% to 65% as the temperature increased from 200℃ to

250℃. At a higher T_s, a decrease in crystalline volume fraction can be observed, may be because of higher H-etching at the film surfaces, by the reactive H radicals.

Fig. 5(b) shows the electrical properties of the films, deposited at different substrate temperatures (T_s). When the T_s were 100℃ and 140℃, the dark conductivity of the films remained around 10^{-10}S/cm indicating an amorphous film. Raman spectra of the films also indicate similar things. When the temperature was over 200℃, the dark conductivity increased rapidly. Here also the photo conductivity did not change much in the temperature range of 100 ~ 250℃ although there was a small increase at 260℃ temperature.

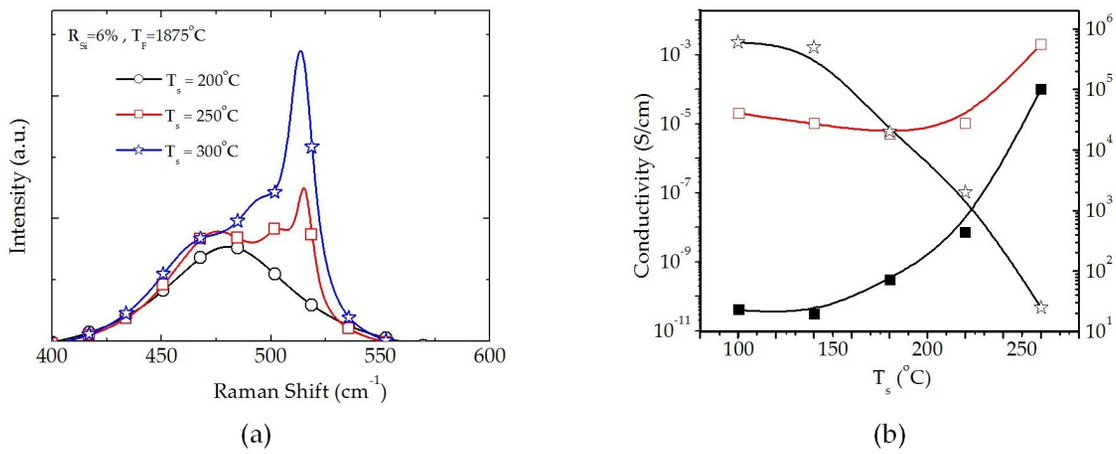

Figure 5. (a) Raman spectra and (b) conductivities of the nc-Si:H films deposited at various substrate temperatures in a HW CVD.

3.7. Analysis of solar cells

The quantum efficiency (QE) is the current generated per unit incident photons, or solar cell current/number of incident photons at a particular wavelength. The spectral response (SR) is the solar cell current (A) per unit incident energy (W) of incident light. The QE and SR is thus related as

$$QE = SR \times (hc / \lambda) \tag{8}$$

where h is Planck's constant, c is the speed and λ is the wavelength of the light. The solar cells were characterized by the QE spectra.

Fig. 6 shows the QE spectra of a-Si:H/nc-Si:H MJ solar cells with various thickness of a-Si:H i-layer of the top cell. As the i-layer thickness was increased from 100 to 300nm, the top cell QE increased while that of the bottom one reduced.

For the QE measurement of a multiple-junction solar cell, a bias light was used to saturate all but one of the cell under investigation. Whereas the light (AM1.5) induced current-volt-

age characteristics (LIV) can give the output J_{sc}, V_{oc}, FF and η of the MJ cell as a whole. From the QE characteristic spectra, one can estimate approximate J_{sc} of the component cells of a MJ cell, and thus it becomes evident that the J_{sc} of a MJ solar cell is limited by the J_{sc} of the top cell. Generally, the limitation comes from any of the component cells, that has the lowest J_{sc}, that acts as the current limiting component of the MJ cell.

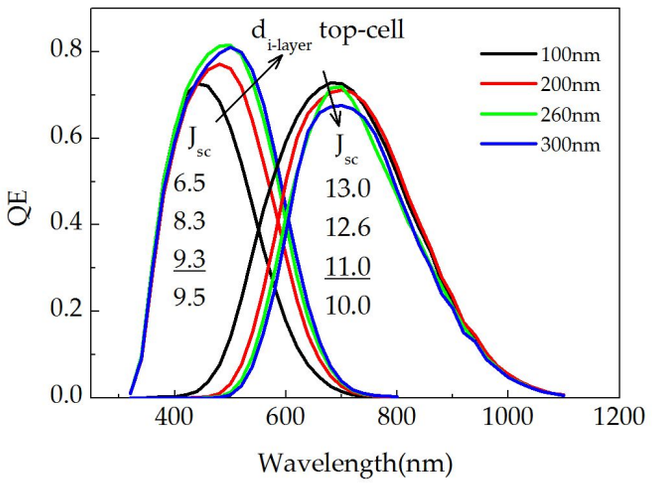

Figure 6. Variation in QE spectra of the top and bottom cells of a double junction cell during current matching experiment.

3.8. Multiple- junction cell, The thickness of top cell

It is important to achieve a current matching among the component cells of a MJ cell. In a best condition, each cell should be designed to have equal J_{sc} having highest possible current density. A few nm thick p μc-Si:H thin film was inserted as a buffer layer between AZO and p-a-$Si_{1-x}C_x$:H window layer of the top cell in order to improve the interface. The thickness of pure a-Si:H absorption layer of the top cell was varied in the range of 100 ~ 300nm by controlling the deposition time and the i-layer of the nc-Si:H bottom cell was kept fixed to 1.7μm. To improve the tunnel junction between the top and bottom cells, less than a few nm thick AZO was deposited by RF magnetron sputtering. The area of the solar cell was 0.36cm^2.

The QE of the top cell increased with increase in i-layer thickness ($d_{i\text{-}layer}$) in the wavelength range of 450 ~ 700nm due to increased absorption of incident light. With a thicker i-layer, the J_{sc} of the top cell increased from 6.5 to 9.5mA/cm^2 but J_{sc} of nc-Si:H bottom cell decreased from 13.0 to 10.0mA/cm^2. This decrease in the J_{sc} of the bottom cell was due to the reduction in QE of the bottom cell in the wavelength longer than 450nm. The V_{oc} of the MJ cell decreased from 1.435 to 1.405 V with the increase in thickness of i-layer of the top cell. The J_{sc} of the MJ solar cell was limited by J_{sc} of the top cell regardless of the top cell thickness. With the increase in top cell thickness, the efficiency increased from 6 to 10%. Fig.7(b,c) shows the change in short circuit current densities of top and bottom cells as top cell thickness was varied.

With increase of thickness of the i-layer, the current of the top cell increased while that of the bottom cell decreased. It seems that a current matching occurs at around 350nm top cell i-layer

http://dx.doi.org/10.5772/51732

thickness, with J_{sc} of 9.5 ~ 10.0mA/cm^2 which is much less than 13mA/cm^2 required for multiple junction solar cell to have an efficiency of above 13%. Unlike the single p-i-n type solar cell, there is no internal reflection effect for light at back electrode (Ag) for a-Si:H/nc-Si:H tandem solar cell so It is important to maximize the collection efficiency around the wavelength range of 500 ~ 700nm. Fig. 7(b) shows J_{sc} of single p-i-n type a-Si:H solar cell and J_{sc} of the top cell of tandem solar cell with different thickness of absorption layers. As mentioned before, J_{sc} of top cell of tandem solar cell was about 1 ~ 2mA/cm^2 lower than that of single p-i-n type solar cell. In a single p-i-n type a-Si:H solar cell, the response in the wavelength range of 500 ~ 700nm is greatly dependent on the reflectivity of back reflector electrode.

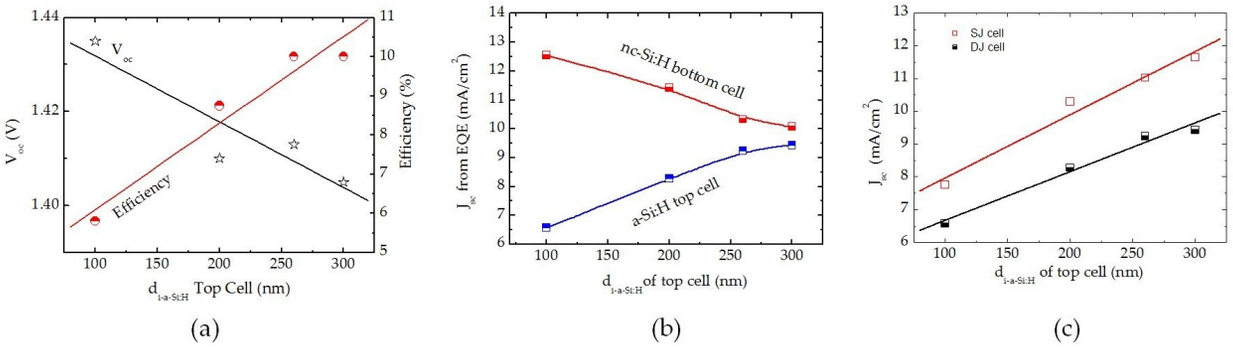

Figure 7. Changes in (a) V_{oc} and (b) J_{sc} of a double junction cell during current matching. (c) Changes in J_{sc} of a single and top cell of a double junction cell with change in top cell i-layer thickness.

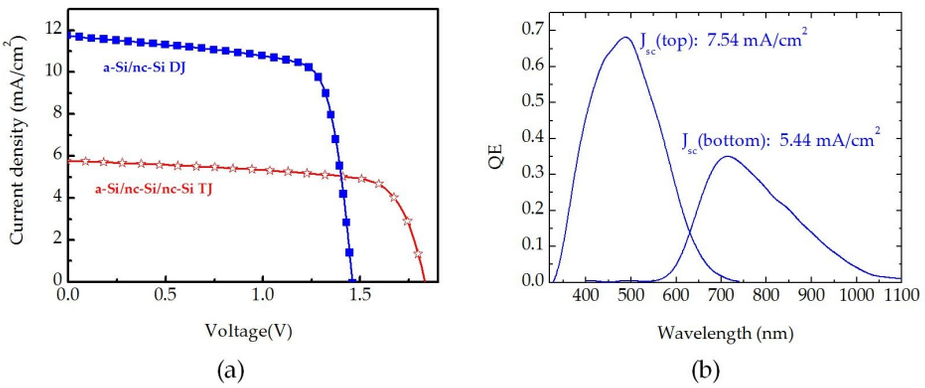

Figure 8. (a) LIV characteristics of a double and triple junction solar cell, (b) QE of top and bottom cells of the triple junction cell.

Fig.8(a) shows the illuminated I-V curves of a-Si:H/nc-Si:H/nc-Si:H triple junction solar cell and a-Si:H/nc-Si:H double junction solar cell. J_{sc} of triple junction solar cell decreased and V_{oc} increased from 1.42 to 1.83V compared with double junction solar cell. Fig.8(b) shows the QE of top and bottom cells of the triple junction solar cell. J_{sc} of the a-Si:H top cell is 7.54 mA/cm^2. The response in the range of 550 ~ 700nm decreases because of the thin layer of 150nm. The J_{sc} of bottom cell with 3.2μm thick nc-Si:H absorption layer is 5.44mA/cm^2 which was close to the

5.72mA/cm^2 measured with solar simulator. It can be said that J_{sc} of triple junction solar cell is limited by the bottom cell and J_{sc} of the nc-Si:H middle cell sould be at least 5.4mA/cm^2.

Even though the bottom cell was composed of 3.2μm thick intrinsic layer, the J_{sc} was low. One of the reasons can be the absorption of incident light by the middle cell. Low haze ratio of the TCO and increased recombination of generated electron hole pair in nc-Si:H absorption layer can also be one of the reasons. In this study, the observed V_{oc} was 1.83V. The reason for the lower V_{oc} is presumed to be the decrease in V_{oc} of the microcrystalline bottom cell. In order to have initial efficiency of over 14%, J_{sc} of unit cells should be at least 9mA/cm^2. For the top cell, it can be done by raising the thickness of the intrinsic a-Si:H layer to ~ 250nm or by increasing the short wavelength QE. However, for the middle and bottom cells, more efforts are needed such as light trapping, improved property of nc-Si:H and development of new intrinsic layer such as nc-SiGe:H [50-52] as well as improvement in the TRJ.

4. Summary

a-Si:H/nc-Si double and a-Si:H/nc-Si:H/nc-Si:H triple junction solar cells have been made and the effects of the top cell thickness and interlayer on the current matching and solar cell characteristics have been investigated. There is a significant impact of the multijunction cell performance on the current matching of the component cells as well as the tunnel junction in between them. When the Si:H top cell thickness was varied from 100 to 300nm, J_{sc} of the top cell increased from 6.5 to 9.5 mA/cm^2. For the bottom cell, J_{sc} decreased from 13.0 to 10.0mA/cm^2 and current matching of the multiple junction solar cell occurred around 330nm resulting in lower J_{sc}. For the top cell of DJ solar cells, unlike the single p-i-n type solar cell, there is no back reflector electrodes (Ag or AZO) present, because of the presence of the bottom cell. So it was difficult to raise the J_{sc} of this cell without increasing its i-layer thickness. The AZO inter-layer was inserted between the top and bottom cells to make the junction like a TRJ. This AZO layer may also work as a partial reflector of unabsorbed light. With a 150nm thick inter-layer, the current gain of the top cell was +1.3mA/cm^2. However, for the nc-Si:H bottom cell, the current loss of -1.77mA/cm^2 occurred due to the reflection and absorption of AZO. By using textured AZO front layer electrode with high haze ratio, it was possible to develop a a-Si:H/nc-Si:H double junction solar cell with V_{oc} of 1.424V, J_{sc} of 12.09mA/cm^2, FF of 72.84%. To develop multiple junction solar cells with initial efficiency over 13%, further studies for improvements on inter-layer property, light trapping and higher response of bottom cell in long wavelength range should be carried out.

For an a-Si/nc-Si/nc-Si triple junction solar cell, 3 units of solar cells were connected in series electrically and optically. Thus, the current matching between each unit was important to get higher efficiency. The a-Si(150nm)/nc-Si(2.0μm)/nc-Si(3.2μm) triple junction solar cell fabricated in this study, showed the V_{oc} of 1.832V, J_{sc} of.773mA/cm^2, FF of 71.41%, and efficiency of 7.49%.

It may be possible to raise the V_{oc} of the MJ cell to 1.95V by optimizing the top cell and the tunnel junction. With this, the FF is also expected to increase. To increase the stabilized effi-

ciency of the top cell, the intrinsic layer thickness should be as thin as possible and improvement in J_{sc} should be carried out through improvement in the short wavelength response. Since the middle and bottom cells absorb light in the relatively long wavelength range, the electrical and optical properties and the thickness of the intrinsic layer need to be optimized. Higher J_{sc} could be obtained by using nc-SiGe:H thin film since its absorption coefficients are higher than those of nc-Si:H thin film.

Author details

S. M. Iftiquar[1*], Jeong Chul Lee[2], Jieun Lee[2], Juyeon Jang[1], Yeun-Jung Lee[1] and Junsin Yi[1,3]

*Address all correspondence to: smiftiquar@gmail.com

1 College of Information and Communication Engineering, Sungkyunkwan University, Republic of Korea

2 Korea Institute of Energy Research, Gajeong-ro, Yuseong-gu, Daejeon, Republic of Korea

3 Department of Energy Science, Sungkyunkwan University, Republic of Korea

References

[1] Tawada, Y., Tsuge, K., Kondo, M., Okamoto, H., & Hamakawa, Y. (1982). Properties and structure of a-SiC:H for high-efficiency a-Si solar cell. *Journal of Applied Physics*, 53, 5273-5281.

[2] Konenkamp, R., Muramatsu, S., Matsubara, S., & Shimada, T. (1992). Space-charge distribution and trapping kinetics in amorphous silicon solar cells. *Applied Physics. Letters*, 60(9), 1120-1122.

[3] Reichman, J. (1981). Collection efficiency of low-mobility solar cells. *Applied Physics Letters*, 38(4), 251-253.

[4] Boer & K. W. (1981). Influence of the electric field on collection efficiencies of solar cells. *Applied Physics Letters*, 38(7), 537-539.

[5] D'Aiello, R. V., Robinson, P. H., & Kressel, H. (1976). Epitaxial silicon solar cells. *Applied Physics Letters*, 28(4), 231-234.

[6] Sinencio, F. S., & Williams, R. (1983). Barrier at the interface between amorphous silicon and transparent conducting oxides and its influence on solar cell performance. *Journal of Applied Physics*, 54(5), 2757-2760.

[7] Banerjee, A., Yang, J., Glatfelter, T., Hoffman, K., & Guha, S. (1994). Experimental study of p layers in ''tunnel'' junctions for high efficiency amorphous silicon alloy multijunction solar cells and modules. *Applied Physics Letters*, 64-1517.

[8] Myong, S. Y., Lim, K. S., & Pears, J. M. (2005). Double amorphous silicon-carbide p-layer structures producing highly stabilized pin-type protocrystalline silicon multi-layer solar cells. *Applied Physics Letters*, 87(3), 193509.

[9] Wang, F., & Schwarz, R. (1993). Characterization of optoelectronic properties of a-$Si1_xC_x$:H films. *Journal of Non-Crystalline Solids*, 164-166, 1039-1042.

[10] Iftiquar, S. M., & Barua, A. K. (1999). Control of the properties of wide bandgap a-SiC : H films prepared by RF PECVD method by varying methane flow rate. *Solar Energy Materials and Solar Cells*, 56, 117-123.

[11] Chaudhuri, P., Ray, S., Batabyal, A. K., & Barua, A. K. (1984). Properties of undoped and p-type hydrogenated amorphous silicon carbide films. *Thin Solid Films*, 121, 233-246.

[12] Yoon, K., Kim, Y., Park, J., Shin, C. H., Baek, S., Jang, J., Iftiquar, S. M., & Yi, J. (2011). Preparation and characterization of p-type hydrogenated amorphous silicon oxide film and its application to solar cell. *Journal of Non-Crystalline Solids*, 357, 2826-2832.

[13] Yoon, S. F., Ji, R., & Ahn, J. (1997). Some effects of boron doping in a-SiC:H films prepared by the ECR-CVD method. *Journal of Non-Crystalline Solids*, 211, 173-179.

[14] Kanbara, T., & Kondo, S. (1991). A new type of amorphous silicon solar cell with high thermal stability. *Japanese Journal of Applied Physics*, 30, 1653-1658.

[15] Park, J. H., Choi, J. B., Kim, H. Y., Lee, K. Y., & Lee, J. Y. (1995). A study on the structural characterization of a-SiC:H films by the gas evolution method. *Thin Solid Films*, 266, 129-132.

[16] Ray, S., Ghosh, S., De Barua, A., & 19, A. K. (1994). Improved quality a-SiC:H films prepared by photo chemical vapour decomposition of silane and acetylene. *Solar Energy Materials and Solar Cells*, 33, 517-531.

[17] Giorgis, F., Ambrosone, G., Coscia, U., Ferrero, S., Mandracci, P., & Pirri, C. F. (2001). Structural and optical properties of a-$Si1_xC_x$:H grown by plasma enhanced CVD. *Applied Surface Science*, 184, 204-208.

[18] Petrich, M. A., Gleason, K. K., & Reimer, J. A. (1987). Structure and properties of amorphous hydrogenated silicon carbide. *Physical Review B*, 36, 9722-9731.

[19] Demichelis, F., Pirri, C. F., & Tresso, E. (1992). Influence of doping on the structural and optoelectronic properties of amorphous and microcrystalline silicon carbide. *Journal of Applied Physics*, 72, 1327-1333.

[20] Bennett, M. S., & Rajan, K. (1990). Stability of multijunction a-Si:H based solar cells. *Journal of Applied Physics*, 67(9), 4161-4166.

http://dx.doi.org/10.5772/51732

[21] Holovsky, J., Bonnet-Eymard, M., Boccard, M., Despeisse, M., & Ballif, C. (2012). Variable light biasing method to measure component I-V characteristics of multi-junction solar cells. *Solar Energy Materials & Solar Cells*, 103, 128-133.

[22] Zheng, X. X., Zhang, X. D., Yang, S. S., Xu, S. Z., Wei, C. C., & Zhao, Y. (2012). Effect of the n/p tunnel junction on the performance of a-Si:H/a-Si:H/mc-Si:H triple-junction solar cells. *Solar Energy Materials & Solar Cells*, 101, 15-21.

[23] Dharmadasa, I. M. (2005). Third generation multi-layer tandem solar cells for achieving high conversion efficiencies. *Solar Energy Materials & Solar Cells*, 85, 293-300.

[24] Hishikawa, Y., Ninomiya, K., Maruyama, E., Kuroda, S., Terakawa, A., Sayama, K., Tarui, H., Sasaki, M., Tsuda, S., & Nakano, S. (1996). Approaches for stable multi-junction a-Si solar cells. *Solar Energy Materials and Solar Cells*, 41/42, 441-452.

[25] Islam, M. N., Pradhan, A., & Kumar, S. (2005). Effects of crystallite size distribution on the Raman-scattering profiles of silicon nanostructures. *Journal of Applied Physics*, 98(6), 024309.

[26] Lebib, S., & Cabarrocas, P. R. I. (2005). Effects of ion energy on the crystal size and hydrogen bonding in plasma-deposited nanocrystalline silicon thin films. *Journal of Applied Physics*, 97(10), 104334.

[27] Bustarret, E., & Hachicha, M. A. (1988). Experimental determination of the nanocrystamne volume fraction in silicon thin films from Raman spectroscopy. *Applied Physics Letters*, 52(20), 1675-1677.

[28] Hu, Z., Liao, X., Diao, H., Cai, Y., Zhang, S., Fortunato, E., & Martins, R. (2006). Hydrogenated p-type nanocrystalline silicon in amorphous silicon solar cells. *Journal of Non-Crystalline Solids*, 352, 1900-1903.

[29] Prasad, K., Finger, F., Dubail, S., Shah, A., & Schubert, M. (1991). Deposition of phosphorus doped microcrystalline silicon below 70 °c at 70 MHz. *Journal of Non-Crystalline Solids*, 137&138, 681-684.

[30] Vetterl, O., Finger, F., Rarius, C., Hapke, P., Houben, L., Kluth, O., Lambertz, A., Muck, A., Rech, B., & Wagner, H. (2000). Intrinsic microcrystalline silicon: A new material for photovoltaics. *Solar Energy Materials & Solar Cells*, 62, 97-108.

[31] Meier, J., Dubail, S., Fluckiger, R., Fischer, D., Keppner, H., & Shah, A. (1994, December). Intrinsic microcrystalline silicon (μc-Si:H)-a promising new thin film solar cell material. Waikoloa, Hawaii, USA. *Proceedings of the 1st IEEE World Conference on Photovoltaic Energy Conversion (WCPEC '94)*, 1, 409-412.

[32] Fischer, D., Dubail, S., Selvan, J. A. A., Vaucher, N. P., Platz, R., Hof, C., Kroll, U., Meler, J., Torres, P., Keppner, H., Wyrsch, N., Goetz, M., Shah, A., & Ufert-D, K. (1996, May 13-17). The "micromorph" solar cell: extending a-si:h technology towards thin film crystalline silicon. Washington, D.C. *25th PVSC*, , 1053-1056.

[33] Tawada, Y., Takada, J., Yamaguchi, M., Yamagishi, H., Nishimura, K., Kondo, M., Hosokawa, Y., Tsuge, K., Nakayama, T., & Hatano, I. (1986). Stability of an amor-

phous SiC/Si tandem solar cell with blocking barriers. *Applied Physics Letters*, 48, 584-586.

[34] Siebke, F., Yata, S., Hishikawa, Y., & Tanaka, M. (1998). Correlation between structure and optoelectronic properties of undoped microcrystalline silicon. *Journal of Non-Crystalline Solids*, 227-230, 977-981.

[35] Wang, D., Liu, Q., Li, F., Qin, Y., Liu, D., Tang, Z., Peng, S., & He, D. (2010). Effect of Ar in the source gas on the microstructure and ptoelectronic properties of microcrystalline silicon films deposited by plasma-enhanced CVD. *Applied Surface Science*, 257, 1342-1346.

[36] He, Y., Yin, C., Cheng, G., Wang, L., Liu, X., & Hu, G. Y. (1994). The structure and properties of nanosize crystalline silicon films. *Journal of Applied Physics*, 75, 797-803.

[37] Brodsky, M. H., Cardona, M., & Cuomo, J. J. (1977). Infrared and Raman spectra of the silicon-hydrogen bonds in amorphous silicon prepared by glow discharge and sputtering. *Physical Review B*, 16(8), 3556-3571.

[38] Baek, S., Lee, J. C., Lee-J, Y., Iftiquar, S. M., Kim, Y., Park, J., & Yi, J. (2012). Interface modification effect between p-type a-SiC: H and ZnO:Al in p-i-n amorphous silicon solar cells. *Nanoscale Research Letters*, 7, 81.

[39] Saleh, R., Munisa, L., & Beyer, W. (2007). Hydrogen induced voids in hydrogenated amorphous silicon carbon (a-SiC:H): Results of effusion and diffusion studies. *Applied Surface Science*, 253, 5334-5340.

[40] Tabata, A., Nakajima, T., Mizutani, T., & Suzuoki, Y. (2003). Preparation of Wide-Gap Hydrogenated Amorphous Silicon Carbide Thin Films by Hot-Wire Chemical Vapor Deposition at a Low Tungsten Temperature. *Japanese Journal of Applied Physics*, 42(2), L10-L12.

[41] Ichihara, T., & Aizawa, K. (1997). Influence of film qualities on noise characteristics of a-Si1xCx:H thin films deposited by PECVD. *Applied Surface Science*, 113/114, 759-763.

[42] Tarui, H., Matsuyama, T., Okamoto, S., Dohjoh, H., Hishikawa, Y., Nakamura, N., Tsuda, S., Nakano, S., Ohnishi, M., & Kuwano, Y. (1989). High-Quality p-Type a-SiC Films Obtained by Using a New Doping Gas of $B(CH_3)_3$. *Japanese Journal of Applied Physics*, 28, 2436-2440.

[43] Folsch, J., Rubel, H., & Schade, H. (1992). Change in bonding properties of amorphous hydrogenated silicon-carbide layers prepared with different gases as carbon sources. *Applied Physics Letters*, 61, 3029-3031.

[44] Lee, C. H., & Lim, K. S. (1998). Boron-doped amorphous diamond like carbon as a new p-type window material in amorphous silicon p-i-n solar cells. *Applied Physics Letters*, 72(1), 106-108.

[45] Tang, Y., & Braunstein, R. (1995). Effects of deposition conditions on transport properties of intrinsic hydrogenated amorphous silicon and hydrogenated amorphous sil-

icon carbide films investigated by the photomixing technique. *Applied Physics Letters*, 66(6), 721-723.

[46] Tawada, Y., Okamoto, H., & Hamakawa, Y. (1981). a-SiC:H/a-Si:H heterojunction solar cell having more than 7.1 % conversion efficiency. *Applied Physics Letters*, 39(3), 237-239.

[47] Tsai, C. C., Anderson, G. B., Wacker, B., Thompson, R., & Doland, C. (1989). Temperature dependance of structure, transport and growth of microcrystalline silicon: Does grain size correlate with transport? *Material Research Society Symposium Proceedings*, 149, 118-123.

[48] Asano, A. (1990). Effects of hydrogen atoms on the network structure of hydrogenated amorphous and microcrystalline silicon thin films. *Applied Physics Letters*, 56, 533-535.

[49] Rajeswaran, G., Kampas, F. J., Vanier, P. E., Sabatini, R. L., & Tafto, J. (1983). Substrate temperature dependence of microcrystallinity in plasma-deposited, boron-doped hydrogenated silicon alloys. *Applied Physics Letters*, 43, 1045.

[50] Kawauchi, H., Isomura, M., Matsui, T., & Kondo, M. (2008). Microcrystalline silicon-germanium thin films prepared by the chemical transport process using hydrogen radicals. *Journal of Non-Crystalline Solids*, 354, 2109-2112.

[51] Nakahata, K., Isomura, M., & Wakisaka, K. (2003). Low-Temperature Crystallization of Poly-SiGe Thin-Films by Solid Phase Crystallization. *Solid State Phenomena*, 93, 231-236.

[52] Matsui, T., Ogata, K., Isomura, M., & Kondo, M. (2006). Microcrystalline silicon-germanium alloys for solar cell application: Growth and material properties. *Journal of Non-Crystalline Solids*, 352, 1255-1258.

IntechOpen

IntechOpen

IntechOpen